ELSEVIER

Physica D 151 (2001) 253–270

PHYSICA D

www.elsevier.com/locate/physd

Solute trapping and the non-equilibrium phase diagram for solidification of binary alloys

Karl Glasner*

Department of Mathematics, University of Utah, 155 S. 1400 E., Salt Lake City, UT 84112-0090, USA

Received 9 June 2000; received in revised form 29 January 2001; accepted 1 February 2001
Communicated by C.K.R.T. Jones

Abstract

A phase field model for the solidification of binary alloys is presented and analyzed. A matched asymptotic approach is used to recover the model's leading order sharp interface motion. Equations for both the solute profile and free energy balance at the interface are derived, demonstrating solute trapping at large growth velocities and leading to a construction of the non-equilibrium phase diagram over a large range of growth conditions. A rigorous understanding of the interfacial conditions is provided, and comparisons are made to existing theories. © 2001 Published by Elsevier Science B.V.

PACS: 68.10.Jy; 82.65.Dp; 64.70.Dv

Keywords: Binary alloys; Phase field models; Solute trapping; Solute drag; Phase diagram

1. Introduction

As a liquid melt composed of two (or more) atomic species solidifies, the resulting solid typically has composition unequal to that of the liquid. This composition depends in part on the local conditions under which growth occurred, in particular on the rapidity of solidification. As a result, the growth conditions largely determine the resulting solid microstructure and its material properties. The goal of this paper is to present a theory which predicts binary alloy composition under non-equilibrium growth conditions.

Sharp interface models for alloy growth rely on two basic elements: a conservation law for mass redistribution, and assumptions about how composition at the interface varies with growth conditions. The continuous growth (CG) model of Aziz and Kaplan [3] is one such approach which specifies material flux and phase change reaction rates at the interface. This theory predicts that the jump in composition between solid and liquid will vanish as the interface velocity becomes large, a phenomenon known as solute trapping. There is considerable experimental evidence for this effect [16,20].

Phase field models offer another approach to understanding phase transition processes, especially under non-equilibrium conditions. Such models have been used extensively to describe solidification of pure materials

* Tel.: +801-268-8216.
E-mail address: glasner@math.utah.edu (K. Glasner).

0167-2789/01/$ – see front matter © 2001 Published by Elsevier Science B.V.
PII: S0167-2789(01)00231-7

[9,18,19,23]. For alloy problems, studies with diffuse phase boundaries date back to the work of Baker and Cahn [4]. Complete phase field models for binary alloys have been developed by Wheeler et al. [25], Caginalp and Xie [7], and Bi and Sekerka [5]. These models have been used in numerical simulation of pattern formation and microstructure evolution [10,11,24]. Alloy models for systems with more than one solid phase have also been developed [12,22,27].

Solute trapping has been predicted in phase field models as a natural consequence of the model's construction. There have been two distinct ways in which this effect has been recovered. The first is to incorporate in the model a description of energy due to large gradients of composition. This approach was first suggested by Wheeler et al. [26], and an asymptotic analysis was undertaken by Charach and Fife [8].

Recently, solute trapping has been reported in models without the addition of solute gradient energy by Ahmad et al. [1] and Kim et al. [17]. Rather than recovering the sharp interface laws as an asymptotic limit of small interface width, their idea is to regard the interface width as finite, and consider instead the limit of large growth velocity. They study one-dimensional solutions and conclude that solute trapping occurs as the mass diffusion length approaches the scale of the diffuse interface thickness.

This paper is similar to the latter studies by not including solute gradient energy. The main result here is that sharp interface laws exhibiting solute trapping can be recovered from the model by asymptotic analysis. In doing this, it is necessary to carefully determine the proper scales of the terms appearing in the equations. In the intermediate velocity regime, the assumed scaling maintains a constant *ratio* of diffusion to interface length scales, so that the sharp interface limit captures the correct interaction between fields.

The main ideas are as follows:

- A model is constructed from a free energy functional, making only a few restrictive assumptions about the constitutive functions which appear.
- A careful asymptotic analysis is conducted, giving a set of necessary conditions which the model's leading order behavior must satisfy.
- The segregation of solute is predicted by a degenerate boundary value problem. A rigorous analysis of this problem is presented, demonstrating solute trapping effects at high velocity.
- The non-equilibrium phase diagram is given by solvability criteria from the asymptotic analysis in conjunction with the solute segregation equation.

The paper begins with a description of the phase field model, proceeds to analyze the leading order behavior for small interface width, and concludes with computational examples which are compared with other studies.

2. Phase field model

The system we are concerned with is an ideal mixture of two species A and B. The model will involve the functions $\phi(x,t)$ and $c(x,t)$, designating the phase of the system and fractional concentration of species B (molar volumes of A and B are presumed to be identical). We will take $\phi = 1$ to be solid and $\phi = -1$ to be liquid. The temperature T of the system will be a specified constant parameter, although it is not hard to incorporate thermal effects as well [5,7].

We start with an assumed form of the total Helmholtz free energy:

$$F(\phi, c, T) = \int \frac{g(\phi)}{a} + \frac{b}{2}|\nabla\phi|^2 + f(\phi, c, T)\,\mathrm{d}x, \tag{2.1}$$

which is the sum of the bulk free energy density $f(\phi, c, T)$ and terms representing the interface free energy. The function $g(\phi)$ is a non-dimensional potential, assumed to be positive and possessing wells at ± 1 so that $g(\pm 1) = 0$.

Dynamic models may be derived from (2.1) as gradient flows (for example, see [5]), or as balances of interfacial stresses [13,14]. Our model will be a generalization of the isothermal alloy models appearing in [1,17,25], taking the form

$$\phi_t = -M_\phi(\phi, c)\frac{\delta F}{\delta \phi}, \tag{2.2}$$

$$c_t = \nabla \cdot \left(M(\phi, c)\nabla \frac{\delta F}{\delta c} \right), \tag{2.3}$$

where M_ϕ, $M > 0$ are solute and phase mobilities, respectively. For simplicity, M_ϕ will be taken to be a constant, and M will depend only on the phase ϕ.

It will be convenient for what follows to write the solute mobility as

$$M(\phi) = \frac{M_{\mathrm{L}} M_{\mathrm{S}}}{q(\phi)M_{\mathrm{L}} + (1 - q(\phi))M_{\mathrm{S}}}, \tag{2.4}$$

where M_{L}, M_{S} are values of mobility in the liquid and solid, respectively, and $q(\phi)$ is a monotone increasing function with $q(1) = 1$, $q(-1) = 0$. Note that this maintains generality by allowing $q(\phi)$ to be otherwise arbitrary.

2.1. Equilibrium interface and constitutive functions

The parameters a and b can be related to the diffuse interface width and surface energy as in Ref. [7]. Ignoring the bulk free energy component in (2.1) for a moment, the equilibrium interface profile will solve the Euler–Lagrange equation

$$b\phi_{xx} - \frac{1}{a}g'(\phi) = 0, \tag{2.5}$$

which may be integrated to give a decreasing interface profile given implicitly by

$$\phi_x(x) = -\sqrt{\frac{2g(\phi(x))}{ab}}. \tag{2.6}$$

This motivates the definition for the interface width

$$\epsilon = \sqrt{ab}. \tag{2.7}$$

The free energy of the equilibrium interface, which is just the surface energy density, is then

$$\sigma = \sqrt{\frac{b}{a}}\int_{-1}^{1} \sqrt{2g(\phi)}\,\mathrm{d}\phi. \tag{2.8}$$

Without loss of generality, we will assume that $\int_{-1}^{1}\sqrt{2g(\phi)} = 1$; the parameters are therefore related by

$$a = \frac{\epsilon}{\sigma}, \qquad b = \epsilon\sigma. \tag{2.9}$$

The bulk free energy density $f(\phi, c, T)$ will be endowed with several standard properties, but will otherwise be considered arbitrary for most of this paper. The interdiffusion potential (the difference of chemical potentials of the two species) is

$$\mu(\phi, c, T) = f_c(\phi, c, T). \tag{2.10}$$

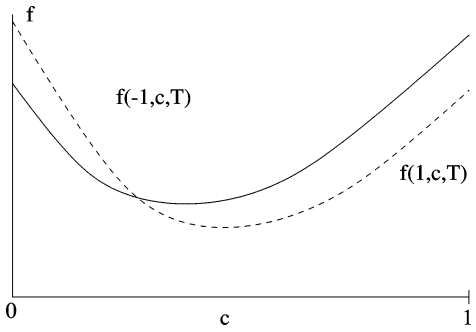

Fig. 1. Typical solid (solid line) and liquid (dashed line) free energy curves at fixed temperature. As the temperature decreases, the liquid curve tends upwards relative to the solid curve.

Without loss of generality, we assume species A has a greater melting temperature than species B. In light of this, we suppose that

$$\frac{\partial \mu}{\partial \phi} = \frac{\partial}{\partial c}\frac{\partial f}{\partial \phi} > 0. \tag{2.11}$$

Additionally, the free energy is convex in c, giving

$$\frac{\partial \mu}{\partial c} > 0. \tag{2.12}$$

We may alternatively regard c as a function of μ and ϕ, writing $c(\phi, \mu, T)$. By the usual relations

$$\frac{\partial \mu}{\partial c}\frac{\partial c}{\partial \mu} = 1, \qquad \frac{\partial \mu}{\partial c}\frac{\partial c}{\partial \phi}\frac{\partial \phi}{\partial \mu} = -1 \tag{2.13}$$

we obtain from (2.11) and (2.12)

$$\frac{\partial c}{\partial \phi} < 0, \qquad \frac{\partial c}{\partial \mu} > 0. \tag{2.14}$$

An example of the free energy function is shown in Fig. 1.

To avoid more notation, we will also use c, μ to denote the values of these quantities, rather than the functional relationships among them. The context will remove any ambiguity which results.

2.2. Dimensionless version

Let X, T, L be characteristic values of length, time and energy scale (the latent heat, for example), respectively. It will also be important to talk about the characteristic velocity $V = X/T$. Rescale in time and space by setting

$$x' = \frac{x}{X}, \qquad t' = \frac{t}{T} \tag{2.15}$$

and define the dimensionless quantities

$$\epsilon' = \frac{\epsilon}{X}, \qquad \alpha = \frac{X^4}{M_\phi L T \epsilon}, \qquad \sigma' = \frac{\sigma X^2}{L}, \qquad f' = \frac{fX^3}{L}, \qquad M'(\phi) = \frac{M(\phi)T}{X^2}. \tag{2.16}$$

We will mostly be interested in the case where mobility in the liquid is much larger than in the solid, so we define the ratio

$$\lambda = \frac{M_{\mathrm{L}}}{M_{\mathrm{S}}}. \tag{2.17}$$

Now set $M'_{\mathrm{L}} = M_{\mathrm{L}} T / X^2$ and write

$$M'_{\mathrm{S}} = \frac{M_{\mathrm{S}} T}{X^2} = \left(\frac{M_{\mathrm{L}}}{\lambda \epsilon V}\right) \epsilon' \equiv \rho \epsilon'. \tag{2.18}$$

Our principal interest is when ρ an $\mathcal{O}(1)$ quantity, which assumes a range of growth velocities which have the characteristic scale

$$V_T = \frac{M_{\mathrm{L}}}{\lambda \epsilon}. \tag{2.19}$$

We shall, however, also consider other scales for ρ in Section 6.

The equations are (dropping the prime notation)

$$\frac{\alpha \epsilon^2}{\sigma} \phi_t = \epsilon^2 \Delta \phi - g'(\phi) - \frac{\epsilon}{\sigma} f_\phi(\phi, c, T), \tag{2.20}$$

$$c_t = \nabla \cdot (M(\phi) \nabla \mu) \tag{2.21}$$

with

$$M(\phi) = \frac{M_{\mathrm{L}} \rho \epsilon}{q(\phi) M_{\mathrm{L}} + (1 - q(\phi)) \rho \epsilon}. \tag{2.22}$$

Note that, provided $q(\phi) \gg \epsilon$, the mobility will be $\mathcal{O}(\epsilon)$. This is a very important aspect of the following asymptotic analysis.

3. Sharp interface limit

To derive the leading order motion of the model, matched asymptotic expansions will be used. It will be assumed that the liquid region $\Omega_{\mathrm{L}}(t; \epsilon) = \{\phi < 0\}$ and the solid region $\Omega_{\mathrm{S}}(t; \epsilon) = \{\phi > 0\}$ are separated by a smooth evolving interface $\Gamma(t; \epsilon)$ which has a smooth, finite limit as $\epsilon \to 0$. There is some local, orthogonal coordinate system (r, s) for which $r(\boldsymbol{x}, t; \epsilon)$ is the signed distance to $\Gamma(t; \epsilon)$ with r positive in the liquid region, and $s(\boldsymbol{x}, t; \epsilon)$ is chosen so that it parameterizes the interface when $r = 0$.

Well away from the interface (when $|r|$ is large in comparison with ϵ), the functions ϕ, c, μ will denote an "outer solution". Each will be expanded in a regular series of powers of ϵ.

We will suppose there is a layer at near the interface which defines an "inner" region, and there we will use the rescaled normal coordinate

$$z = \frac{r}{\epsilon}. \tag{3.1}$$

We will use the notation $\Phi = \phi(z, s, t)$, $C = c(z, s, t)$ and $\mathcal{M} = \mu(z, s, t)$ for the inner region solutions, and each of these will also have a regular expansion in powers of ϵ.

Written in the (z, s, t) coordinates, the equations are

$$\epsilon^2 \frac{\alpha}{\sigma}(\Phi_t + s_t \Phi_s) + \epsilon \frac{\alpha}{\sigma} r_t \Phi_z = \Phi_{zz} - g'(\Phi) + \epsilon \left[\Delta r \Phi_z - \frac{1}{\sigma} f_\phi(\Phi, C, T)\right] + \epsilon^2 [\Delta s \Phi_s + |\nabla s|^2 \Phi_{ss}], \tag{3.2}$$

$$\epsilon^2(C_t + s_t C_s) + \epsilon r_t C_z = (M(\phi)\mathcal{M}_z)_z + \epsilon \Delta r M(\phi)\mathcal{M}_r + \epsilon^2[M(\phi)\Delta s \mathcal{M}_s + |\nabla s|^2 (M(\phi)\mathcal{M}_s)_s]. \tag{3.3}$$

The interface velocity V and curvature κ also need to be expanded in powers of ϵ. We will, however, only be concerned with their leading order terms, which are related to the moving, curvilinear coordinates by the expressions

$$\kappa_0 = \Delta r, \qquad V_0 = -r_t. \tag{3.4}$$

It is implicit in the way that the characteristic scales were chosen that V_0 is an $\mathcal{O}(1)$ quantity.

3.1. Matching and auxiliary conditions

Where each region overlaps the other, different expansions must describe the same function (a detailed explanation is provided by Caginalp and Fife [6]). Suppose $u(r, s, t)$ is some outer solution defined for $r > 0$ and $U(z, s, t)$ some inner region solution. By a Taylor expansion

$$u(r, s, t) = u_0(\epsilon z, s, t) + \delta u_1(\epsilon z, s, t) + \cdots = u_0(0_+, s, t) + \delta[u_1(0_+, s, t) + u_0'(0_+, s, t)z] + \cdots, \tag{3.5}$$

where primes denote derivatives with respect to r and 0_+ denotes limits from the right. By taking $\delta \to 0$ while simultaneously taking z large we obtain

$$\lim_{z \to \pm\infty} U_0(z, s, t) = u_0(0_\pm, s, t) \tag{3.6}$$

and

$$U_1(z, s, t) \sim u_0'(0_+, s, t)z + u_1(0_+, s, t) + \mathrm{o}(1), \quad z \to \pm\infty. \tag{3.7}$$

There is special matching condition which we shall draw attention to. Anticipating that ϕ is not close to -1 in the inner region, the normal component of flux $J_\mathrm{n} = M(\phi)\mu_r$ therefore has the expansion

$$J_\mathrm{n} = \frac{\rho}{q(\Phi)} \frac{\partial \mathcal{M}_0}{\partial z}(z, s, t) + \mathcal{O}(\epsilon). \tag{3.8}$$

In the outer region, we anticipate ϕ will be -1 up to transcendentally small corrections, so that the flux may also be written as

$$J_\mathrm{n} = M_\mathrm{L} \frac{\partial \mu_0}{\partial r}(r, s, t) + \mathcal{O}(\epsilon). \tag{3.9}$$

Matching the expansions in (3.8) and (3.9) as before gives

$$\lim_{z \to \infty} \frac{\rho}{q(\Phi_0)} \frac{\partial \mathcal{M}_0(z, s, t)}{\partial z} = M_\mathrm{L} \frac{\partial \mu_0(0_+, s, t)}{\partial r}. \tag{3.10}$$

As a final note, by the definition of Γ, Φ must satisfy $\Phi(0, s, t) = 0$ at each order of the expansion, giving the series of conditions

$$\Phi_0(0, s, t) = 0, \qquad \Phi_1(0, s, t) = 0, \text{ etc.} \tag{3.11}$$

3.2. Leading order solutions

In the outer region, ϕ solves $g'(\phi_0) = 0$, which means $\phi_0 = \pm 1$, corresponding to each bulk phase. In the liquid region Ω_L, the leading order concentration will solve a diffusion equation

$$(c_0)_t = M_\mathrm{L} \Delta \mu_0(-1, c_0) \tag{3.12}$$

and in the solid region Ω_S, c_0 is simply constant in time:

$$(c_0)_t = 0. \tag{3.13}$$

In the inner region, the phase profile solves

$$(\Phi_0)_{zz} - g'(\Phi_0) = 0 \tag{3.14}$$

with boundary conditions $\Phi(-\infty) = 1$ and $\Phi(\infty) = -1$. This equation is like Eq. (2.5), and has a unique monotonically decreasing solution satisfying $\Phi_0(0) = 0$. For example, if $g(\phi) = \frac{1}{2}(1-\phi^2)^2$ then $\Phi_0(z) = -\tanh(z)$.

In expanding Eq. (3.3), the mobility must be expanded in ϵ to give

$$M(\phi) = \epsilon \frac{\rho}{q(\phi)} + \mathcal{O}(\epsilon^2). \tag{3.15}$$

For this reason, the leading order solute profile will depend on the velocity:

$$-V_0(C_0)_z = \left(\frac{\rho}{q(\Phi_0)} (\mathcal{M}_0)_z \right)_z. \tag{3.16}$$

After integrating once, the constant of integration can be found by taking the limit $z \to -\infty$ and using an outer–inner matching condition. We obtain

$$V_0(c_S - C_0) = \frac{\rho}{q(\Phi_0)} (\mathcal{M}_0)_z, \tag{3.17}$$

where $c_S \equiv c(0_-, s, t)$, the solute concentration just on the liquid side of the interface. Eq. (3.17) governs the segregation of solute across the interface; it will be discussed extensively in the next section. For now, we assume that it has a unique solution.

Taking the limit $z \to \infty$ and using the flux matching condition (3.10) gives the solvability condition

$$V_0(c_L - c_S) = -M_L \left. \frac{\partial \mu_0}{\partial n} \right|_{\Gamma_L}, \tag{3.18}$$

where Γ_L refers to evaluation on the liquid side of the interface. This is the Stefan-type condition for conservation of mass across a moving discontinuity.

3.3. Solutions at order $\mathcal{O}(\epsilon)$

At next order, the inner ϕ equation reads

$$\mathcal{L}\Phi_2 = \left(\kappa_0 + \frac{\alpha}{\sigma} V_0 \right) (\Phi_1)_z - \frac{1}{\sigma} f_\phi(\Phi_0, C_0, T), \tag{3.19}$$

where the self-adjoint operator $\mathcal{L} = \mathrm{d}^2/\mathrm{d}z^2 - g''(\Phi_0)$. Multiplying by $(\Phi_0)_z$ and integrating, we obtain as a solvability condition

$$(\sigma\kappa_0 + \alpha V_0) \int_{-\infty}^{\infty} (\Phi_0)_z^2 \, \mathrm{d}z = \int_{-\infty}^{\infty} f_\phi(\Phi_0, C_0, T)(\Phi_0)_z \, \mathrm{d}z = [f(\Phi_0, C_0, T)]_{-\infty}^{\infty} - \int_{-\infty}^{\infty} \mathcal{M}_0 (C_0)_z \, \mathrm{d}z. \tag{3.20}$$

Using integrating by parts,

$$\int_{-\infty}^{\infty} (C_0)_z \mathcal{M}_0 \, \mathrm{d}z = \mu_L(c_L - c_S) + \frac{\rho}{V_0} \int_{-\infty}^{\infty} \frac{(\mu_0)_z^2}{q(\phi)} \, \mathrm{d}z \equiv \mu_L(c_L - c_S) + J. \tag{3.21}$$

Since $\int_{-\infty}^{\infty}(\Phi_0)_z^2\,\mathrm{d}z = 1$, Eq. (3.20) may be written as

$$\{f(-1, c_\mathrm{L}, T) - f(1, c_\mathrm{S}, T) - \mu_\mathrm{L}(c_\mathrm{L} - c_\mathrm{S}) - \sigma\kappa_0\} - J = \alpha V_0. \tag{3.22}$$

A discussion of this will be carried out in Section 5.

3.4. Free boundary problem

The previous analysis yields a free boundary problem for the evolution of the phase interface. Let V, κ denote the normal interface velocity and curvature and let c_L be the limit of $c(x, t)$ at the interface from the liquid side. The equations which dictate the flow of material are

$$c_t = M_\mathrm{L}\Delta\mu(c), \qquad x \in \Omega_\mathrm{L}, \tag{3.23}$$

$$V(c_\mathrm{L} - c_\mathrm{S}) = -M_\mathrm{L}\left.\frac{\partial\mu}{\partial n}\right|_{\Gamma_\mathrm{L}}. \tag{3.24}$$

Eq. (3.17) will give a condition relating the interface velocity to the local compositions, which takes the form

$$c_\mathrm{S} = h_1(c_\mathrm{L}, V). \tag{3.25}$$

The free energy balance (3.22) will impose another constraint of the form

$$h_2(c_\mathrm{L}, c_\mathrm{S}, T, V, \kappa) = 0. \tag{3.26}$$

The interface concentrations can be found as functions of local conditions by solving (3.25) and (3.26) simultaneously.

It may be that (3.23)–(3.26) does not always posses a solution; indeed, we will see that there are growth conditions for which we can find no solution at all for the interface composition. This is just a reflection of the fact that the analysis made certain assumptions about the sizes of the quantities involved. When those assumptions are violated, we must replace the above free boundary problem with a different one. This is discussed further in Section 6.

4. Solute segregation

Properties of segregation equation (3.17) will now be discussed in the theorem which follows. In short, the theorem states that the difference between liquid and solid solute concentrations decreases monotonically as the interface velocity increases. Furthermore, complete solute trapping, where the liquid and solid concentrations are equal, occurs in the limit of large velocity.

To simplify notation, set $\mu = \mathcal{M}_0$, $\phi = \Phi_0$, $c = C_0$, and $v = V_0/\rho$ so that (3.17) may be rewritten as

$$\mu_z = vq(\phi)[c_\mathrm{S} - c(\phi, \mu)] \tag{4.1}$$

which has the boundary condition

$$\lim_{z\to-\infty}\mu(z) = \mu_\mathrm{S} = \mu(1, c_\mathrm{S}). \tag{4.2}$$

Eq. (3.14) may be integrated to obtain

$$\phi_z = -\sqrt{2g(\phi)}, \tag{4.3}$$

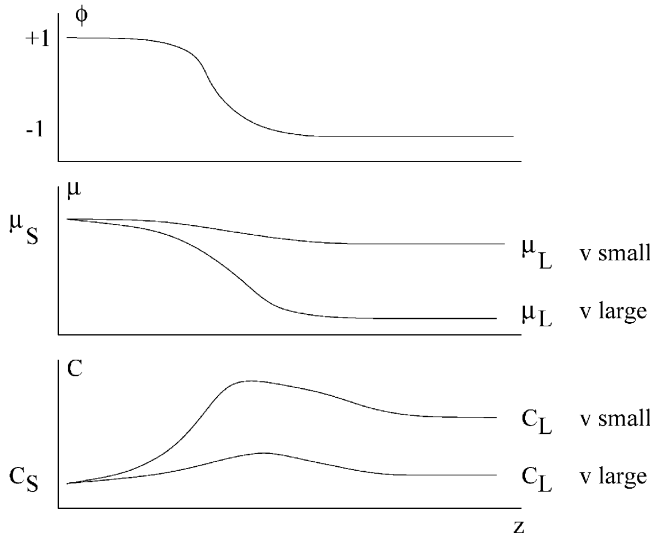

Fig. 2. A qualitative picture of the inner solution profiles for ϕ, μ and c. As v increases, the solute profile becomes flatter, and its asymptotic limits approach a common value.

whose solution is made unique by specifying

$$\phi(0) = 0, \tag{4.4a}$$

$$\lim_{z\to\pm\infty} \phi(z) = \mp 1. \tag{4.4b}$$

Eqs. (4.1)–(4.4) will uniquely determine a solution for $c(z)$ for a given value of the solid solute concentration c_S.

For a given value of v, define

$$\mu_L(v) = \lim_{z\to\infty} \mu(z), \qquad c_L(v) = c(-1, \mu_L) \tag{4.5}$$

to be the liquid values of μ and c. When the velocity is small, $\mu(z)$ will be approximately constant, and the liquid concentration will approach the value

$$c_L^* = c(-1, \mu(1, c_S)). \tag{4.6}$$

A schematic representation of the profiles for ϕ, μ and c and their relationship to the outer solution values is shown in Fig. 2. The solutions to (4.1)–(4.4) are all qualitatively similar to this picture, and their properties will be verified rigorously.

The theorem relies on two technical assumptions, that there exist positive constants C_1, C_2 so that

$$\frac{q(\phi)}{\sqrt{g(\phi)}} > C_1 > 0 \tag{4.7}$$

and

$$\lim_{\phi\to 1} \frac{g'(\phi)}{\sqrt{g(\phi)}} = -C_2 < 0. \tag{4.8}$$

Properties of segregation equation are now summarized.

Theorem 1. *The problem* (4.1)–(4.4) *has a unique solution satisfying the following:*

1. $\mu(z)$ *monotonically decreases in* z,
2. $c_{\mathrm{L}}^* \geq c_{\mathrm{L}}(v) \geq c_{\mathrm{S}}$,
3. $c(z)$ *is increasing as a function of* c_{S},
4. $c_{\mathrm{L}}(v)$ *is decreasing as a function of* v,
5. *The solute profile has the bound*

$$c(z) - c_{\mathrm{S}} \leq \frac{\mathit{constant}}{v}. \tag{4.9}$$

6. *As* $v \to \infty$, $c_{\mathrm{L}} \to c_{\mathrm{S}}$.

Proof. Linearizing Eqs. (4.1) and (4.3) about the equilibrium $(\phi, \mu) = (1, \mu_{\mathrm{S}})$ gives the system

$$\begin{pmatrix} \phi - 1 \\ \mu - \mu_{\mathrm{S}} \end{pmatrix}_z = \begin{pmatrix} C_2 & 0 \\ -vc_\phi(1, \mu_{\mathrm{S}}) & -vc_\mu(1, \mu_{\mathrm{S}}) \end{pmatrix} \begin{pmatrix} \phi - 1 \\ \mu - \mu_{\mathrm{S}} \end{pmatrix}, \tag{4.10}$$

where C_2 is defined in (4.8). Since $\partial c/\partial \mu > 0$, this equilibrium is hyperbolic, and has a one-dimensional unstable manifold U tangent to the line

$$\mu - \mu_{\mathrm{S}} = \frac{-c_\phi(1, \mu_{\mathrm{S}})}{c_\mu(1, \mu_{\mathrm{S}}) + C_2 v^{-1}}(\phi - 1) \tag{4.11}$$

in the (ϕ, μ) plane. Pick any point on U, (ϕ^*, u^*) with $\phi^* < 1$. The forward and backward solutions to the initial value problem (4.1) and (4.3) with initial data $(\phi(0), u(0)) = (\phi^*, u^*)$ will give a solution satisfying (4.2). Condition (4.4a) can be satisfied by an appropriate translation of this solution. Uniqueness follows from the fact that any solution satisfying (4.2), (4.4b) must intersect U.

Proof of (a): Let $\pi(z) = \mu_z$. By differentiating (4.1), it is seen that π solves

$$\pi_z + Q(z)\pi = -vq(\phi)\left(\frac{\partial c}{\partial \phi}\right)\phi_z < 0, \tag{4.12}$$

where

$$Q(z) = vq(\phi)\frac{\partial c}{\partial \mu} - \frac{q(\phi)_z}{q(\phi)} > 0. \tag{4.13}$$

Define the positive integrating factor $K(z) = \exp(\int_0^z Q(z')\,\mathrm{d}z')$. Multiplying by K and integrating (4.12) from $-\infty$ to z gives

$$\pi(z)K(z) < 0. \tag{4.14}$$

Proof of (b): Using part (a) and Eq. (4.1), $\mathrm{d}\mu/\mathrm{d}z > 0$ implies $c(z) > c_{\mathrm{S}}$ for all z. The other inequality is verified by observing that

$$c_{\mathrm{L}} = c(-1, \mu_{\mathrm{L}}) < c(-1, \mu_{\mathrm{S}}) = c_{\mathrm{L}}^*. \tag{4.15}$$

Proof of (c): Let $c_1(z), c_2(z)$ be solutions (given implicitly via μ) for the values $c_{\mathrm{S}} = c_{\mathrm{S}}^1, c_{\mathrm{S}}^2$, respectively, and suppose

$$c_{\mathrm{S}}^1 < c_{\mathrm{S}}^2. \tag{4.16}$$

In general the function $c(\phi(z), \mu(z))$ will solve the equation

$$c_z = \frac{\partial c}{\partial \mu}\mu_z + \frac{\partial c}{\partial \phi}\phi_z, \tag{4.17}$$

which, using (4.1) takes the form

$$c_z = c_S u(c, z) + w(c, z), \tag{4.18}$$

where $u(c, z) > 0$. As $z \to -\infty$, it must be that $c_1(z) < c_2(z)$. Now assume there is some minimal z^* for which $c_1(z^*) = c_2(z^*)$. Then

$$(c_1)_z(z^*) = c_S^1 u(c_1(z^*), z^*) + w(c_1(z^*), z^*) < c_S^2 u(c_2(z^*), z^*) + w(c_2(z^*), z^*) = (c_2)_z(z^*), \tag{4.19}$$

which is impossible since $c_1(z)$ must have approached $c_2(z)$ from below.

Proof of (d): Let $v_1 < v_2$, but suppose

$$c_L(v_1) < c_L(v_2). \tag{4.20}$$

We may regard ϕ as the independent variable, and $\mu(\phi)$ solves

$$\frac{d\mu}{d\phi} = \frac{vq(\phi)}{\sqrt{2g(\phi)}}[c(\phi, \mu) - c_S]. \tag{4.21}$$

Consider solutions $\mu_{1,2}$ to (4.21) with $v = v_{1,2}$ and initial data $\mu_{1,2}(-1) = \mu(-1, c_L(v_{1,2}))$. We claim that $\mu_1(\phi) < \mu_2(\phi)$ for all $\phi \in (-1, 1)$. Using $\partial\mu/\partial c > 0$ and assumption (4.20), this must be the case at $\phi = -1$. Suppose that there is some minimal ϕ^* at which $\mu_1 = \mu_2$. At this point,

$$\frac{d\mu_1}{d\phi} = \frac{v_1 q(\phi^*)}{\sqrt{2g(\phi^*)}}[c(\phi^*, \mu_1(\phi^*)) - c_S] < \frac{v_2 q(\phi^*)}{\sqrt{2g(\phi^*)}}[c(\phi^*, \mu_2(\phi^*)) - c_S] = \frac{d\mu_2}{d\phi}. \tag{4.22}$$

But this is impossible since μ_1 approaches μ_2 from below, establishing the claim.

Notice by the form of the linear unstable manifold (4.11), that near $\phi = +1$, we must have $\mu_1 > \mu_2$. This contradicts the claim and proves (c).

Proof of (e): First we show a lower bound on $\mu(z)$. Since $c(\phi, \mu) > c_S$,

$$\mu(\phi, c) = \mu(\phi, c(\phi, \mu)) > \inf_{\phi \in [-1,1]} \mu(\phi, c_S). \tag{4.23}$$

Since μ also has an upper bound of μ_S, it follows that μ, c and their partial derivatives are bounded independently of v.

Set $C(z) = c(z) - c_s$, which solves

$$C_z + vQ(z)C = P(z), \tag{4.24}$$

where $Q(z) = q(\phi)(\partial c/\partial\mu)$ and $P(z) = (\partial c/\partial\phi)\phi_z$. Introducing the integration factor

$$K(z) = \exp\left(v\int_0^z Q(z')\,dz'\right) \tag{4.25}$$

and noting that $\lim_{z\to-\infty} K(z) = 0$, we may integrate (4.24) to obtain

$$C(z) = \int_{-\infty}^z R(z, z')P(z')\,dz' = \frac{1}{v}\int_{-\infty}^z \frac{\partial R}{\partial z'}(z, z')\frac{P(z')}{Q(z')}\,dz', \tag{4.26}$$

where

$$R(z, z') = \exp\left[v\left(\int_0^{z'} Q(z'')\,dz'' - \int_0^z Q(z'')\,dz''\right)\right]. \tag{4.27}$$

Then observe that

$$\frac{P(z)}{Q(z)} = \frac{(\partial c/\partial \phi)\phi_z}{(\partial c/\partial \mu)q(\phi)} \tag{4.28}$$

is bounded independently of v because of (4.7) and the fact that $\partial c/\partial \mu$ is uniformly bounded away from zero. We have the estimate

$$C(z) \leq \frac{\text{constant}}{v}\int_{-\infty}^{z} \frac{\partial R}{\partial z'}(z, z')\,\mathrm{d}z' = \frac{\text{constant}}{v}. \tag{4.29}$$

Proof of (f): This follows readily from (e). □

5. The non-equilibrium phase diagram

One of our aims is to predict the local segregation of solute at the interface given the local temperature, interface velocity and curvature. In doing so it will be necessary to solve the segregation equation (3.17) and the interface condition (3.22) simultaneously.

We first discuss the meaning of (3.22). The term in brackets is the change in free energy upon solidification of a *curved* interface. The integral J may be identified with an effect known as solute drag, which has appeared in many theories of rapid alloy solidification [1,4,15,17]. This is the component of free energy change which drives solute redistribution *instead* of solidification. The difference of these terms is the free energy which is used to drive the solidification process, which in our case is exactly proportional to the interface velocity, due to our choice of a constant inverse phase mobility α.

We first consider limiting cases for growth velocity to obtain a better understanding of the interface conditions.

5.1. Slow interfaces

Formally setting $V_0 = \kappa_0 = 0$, we obtain from Eq. (3.17) that $\mathcal{M}_0$ is a constant. Therefore relation (3.22) reduces to

$$f(-1, c_\mathrm{L}, T) - f(1, c_\mathrm{S}, T) = \mathcal{M}_0(c_\mathrm{L} - c_\mathrm{S}). \tag{5.1}$$

For given temperature T, the relations

$$\frac{\partial f}{\partial c}(1, c_\mathrm{L}, T) = \mathcal{M}_0 = \frac{\partial f}{\partial c}(1, c_\mathrm{S}, T) \tag{5.2}$$

together with Eq. (5.1) uniquely determine c_L, c_S and $\mathcal{M}_0$. This is simply the usual common tangent construction for equilibrium solute partitioning.

5.2. Fast interfaces

We obtain from the estimate (4.9) that

$$(c_\mathrm{L} - c_\mathrm{S})\mu_\mathrm{L} + J < (\text{constant})V_0^{-1}. \tag{5.3}$$

Then for large velocities, the conditions for a flat interface are asymptotically

$$f(-1, c_\mathrm{L}, T) = f(1, c_\mathrm{S}, T) + \alpha V_0, \tag{5.4}$$

$$c_\mathrm{L} = c_\mathrm{S}. \tag{5.5}$$

Provided αV_0 is negligible, then condition (5.4) simply says that the interface solute concentration lies on the T_0-line, where solid and liquid free energies are the same. On the other hand, as the velocity increases and the αV_0 term becomes appreciable, the interface temperature must fall significantly so as to enlarge the separation between the solid and liquid free energies (see Fig. 1). This crossover of behavior was reported by Aziz and Boettinger [2] for the continuous growth model as well.

5.3. Existence of solutions

It may be that (3.17) and (3.22) admit no solutions for some configurations:

- If T is outside the "two phase" region, which is that between the melting temperatures of the two species, then the graph of $f(-1, c, T)$ will lie entirely above or below the graph of $f(1, c, T)$. For example, if the temperature is less than both melting temperatures, then solid is always thermodynamically preferred, i.e.

$$f(1, c, T) < f(-1, c, T) \tag{5.6}$$

  for all c. In this case both the common tangent and the T_0-line solution do not exist.
- If the velocity is particularly large, then it may be that no solution to (5.4) exists simply because the graphs of both sides do not intersect. If the interface curvature is rather large, a similar situation may occur.

It should be noted that the above considerations do not represent a breakdown in the model, but rather a failure of the asymptotics to capture the true behavior at the interface. In the next section, we amend the asymptotic analysis to include alternative scales which will lead to solvable interface conditions.

As a way of understanding the interface conditions, imagine that c_S is given. Let $c(z; c_S)$ be the corresponding solute profile given by solving (4.1)–(4.4). Define the function

$$E(c_S) = \int_{-\infty}^{\infty} f_\phi(\Phi_0, c(z; c_S), T)(\Phi_0)_z \, dz - G, \tag{5.7}$$

where $G = \sigma\kappa_0 + \alpha V_0$. Comparing with (3.20), it follows that roots of $E(c_S)$ correspond to solutions of the system (3.17) and (3.22). We can now characterize when a unique solutions exists.

Theorem 2. *Let V_0, κ_0, T be given. The function $E(c_S)$ is decreasing, and therefore if*

$$E(0) \geq 0, \qquad E(1) \leq 0 \tag{5.8}$$

there is a unique c_S^* solving $E(c_S^*) = 0$.

Proof. Let c_1, c_2 be two values of c_S for which $c_1 > c_2$. Using Theorem 1(c) and the property $\partial\mu/\partial\phi > 0$ gives

$$\begin{aligned} f_\phi(\phi, c(z; c_1), T) &= \int_0^{c(z;c_1)} \frac{\partial\mu}{\partial\phi}(\phi, c, T)\, dc + f(\phi, 0, T) > \int_0^{c(z;c_2)} \frac{\partial\mu}{\partial\phi}(\phi, c, T)\, dc + f(\phi, 0, T) \\ &= f_\phi(\phi, c(z; c_2), T), \end{aligned} \tag{5.9}$$

which results in

$$E(c_1) = \int_{-\infty}^{\infty} f_\phi(\Phi_0, c(z; c_1), T)(\Phi_0)_z \, dz - G < \int_{-\infty}^{\infty} f_\phi(\Phi_0, c(z; c_2), T)(\Phi_0)_z \, dz - G = E(c_2) \tag{5.10}$$

so E must be a decreasing function. The existence of a unique root follows from the intermediate value theorem. □

6. Alternative scales

We have noted a breakdown in the asymptotic solution in certain regimes, especially when the velocity becomes particularly large. It is therefore necessary to consider different scales of parameters and repeat the asymptotic analysis with these changes.

6.1. Rapid, diffusionless growth

The first case we consider is that where the growth velocity is large enough so that

$$\rho = \mathcal{O}(\epsilon). \tag{6.1}$$

The segregation of solute (3.17) now satisfies at leading order

$$-V_0(C_0)_z = 0. \tag{6.2}$$

The interface composition is the constant value c_{L}, representing complete solute trapping. The free energy balance (3.22) is now

$$\alpha V_0 + \sigma\kappa_0 = f(-1, c_{\mathrm{L}}, T) - f(1, c_{\mathrm{L}}, T). \tag{6.3}$$

The important difference is that the Stefan condition (3.18) becomes

$$\left.\frac{\partial \mu_{\mathrm{L}}}{\partial n}\right|_{\Gamma_{\mathrm{L}}} = 0$$

which is the same as requiring $\partial c/\partial n = 0$ on the liquid side of the interface. Notice that there is no constraint put on the velocity by this condition. Therefore, we should interpret (6.3) as an expression for the *velocity*, rather than for interfacial composition as in Eq. (5.4).

The resulting free boundary problem is

$$c_t = M_{\mathrm{L}}\Delta c, \qquad x \in \Omega_{\mathrm{L}}, \tag{6.4}$$

$$\left.\frac{\partial c}{\partial n}\right|_{\Gamma_{\mathrm{L}}} = 0, \tag{6.5}$$

$$V = \frac{1}{\alpha}(f(-1, c_{\mathrm{L}}, T) - f(1, c_{\mathrm{L}}, T) - \sigma\kappa_0). \tag{6.6}$$

This describes "diffusionless" growth, where diffusion in the liquid side is unnecessary to drive the phase change.

As an example, we might imagine that the liquid side concentration is uniform, so that the interface motion is given by a simple law of the form

$$V = -A\kappa + B, \quad A, B > 0. \tag{6.7}$$

This is a well-known geometric model for crystal growth [21].

6.2. Near equilibrium growth

Suppose now that the velocity scale was small enough so that

$$\rho = \mathcal{O}(\epsilon^{-1}). \tag{6.8}$$

In this case, the non-dimensional diffusion is not small at the interface. Eq. (3.17) will change to yield $\mathcal{M}_0 =$ constant, which means that no solute trapping will occur, and the interface concentrations will be given by their equilibrium values by solving (5.1) and (5.2). The particular free boundary problem whose results has been discussed before [7,25], so we will not write it here.

7. Computational example

For purposes of comparison to other studies, a particular example will be used. The specific model follows that of Ref. [1], with physical parameters appropriate for a Ni–Cu alloy.

The bulk free energy density is

$$f(\phi, c, T) = cf_{\mathrm{B}}(\phi, T) + (1-c) f_{\mathrm{A}}(\phi, T) + \frac{RT}{v_m} I(c), \tag{7.1}$$

where $I(c) = c \ln c + (1-c)\ln(1-c)$ is related to the entropy of mixing. The free energies for the individual species are

$$f_{\mathrm{A,B}} = L_{\mathrm{A,B}} \frac{T - T_{\mathrm{A,B}}}{T_{\mathrm{A,B}}} p(\phi), \tag{7.2}$$

where $L_{\mathrm{A,B}}$ are the latent heats, $T_{\mathrm{A,B}}$ the melting temperatures and $p(\phi) = \frac{3}{4}(\phi - \phi^3)$. The choices we make for g, q are

$$g(\phi) = \tfrac{9}{32}(1-\phi^2)^2, \qquad q(\phi) = \tfrac{1}{2}(\phi + 1). \tag{7.3}$$

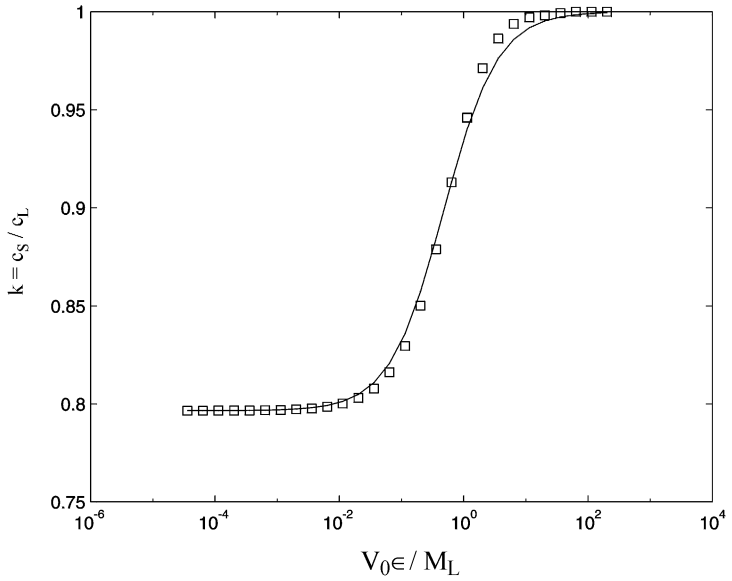

Fig. 3. The segregation coefficient $k = c_{\mathrm{S}}/c_{\mathrm{L}}$ as a function of the non-dimensional growth velocity $V_0\epsilon/M_{\mathrm{L}}$. The squares are solutions to the interface conditions. The solid line is a least-squares fit of the solute trapping function of Aziz et al. (7.8).

The parameter α may be related to the kinetic mobility by considering pure species A only. A one-dimensional traveling wave solution may be sought which solves

$$\epsilon^2\phi_{xx} + \epsilon^2 V\frac{\alpha}{\sigma} + g'(\phi) + \frac{\epsilon}{\sigma}\frac{\partial f_A}{\partial \phi} = 0. \tag{7.4}$$

Multiplying this by ϕ_x and integrating gives

$$\epsilon V\alpha\int_{-\infty}^{\infty}\phi_x^2\,\mathrm{d}x = L_A\frac{T_A - T}{T_A}. \tag{7.5}$$

Near equilibrium, $\int_{-\infty}^{\infty}\phi_x^2\,\mathrm{d}x \approx \epsilon^{-1}$, so the velocity is

$$V = \tilde{\mu}(T_A - T), \tag{7.6}$$

where the kinetic coefficient $\tilde{\mu} = L_A/(T_A\alpha)$ is known experimentally.

The computation of c_S and c_L followed the construction given in Theorems 1 and 2. The unique root of the functional (5.7) was found by a simple bisection method with c_S as the independent variable. Computing this functional relied on knowing the entire solute profile $c(z)$, which was determined by simply integrating Eqs. (4.1)–(4.4) numerically.

The unique solute profile determines the segregation coefficient

$$k = \frac{c_S}{c_L}. \tag{7.7}$$

This was evaluated for different solidification velocities and assuming a flat ($\kappa = 0$) interface. Fig. 3 shows the computed values of k versus the non-dimensional velocity $V' = V_0\epsilon/M_L$. As V' increased beyond about 10^3, solutions ceased to exist.

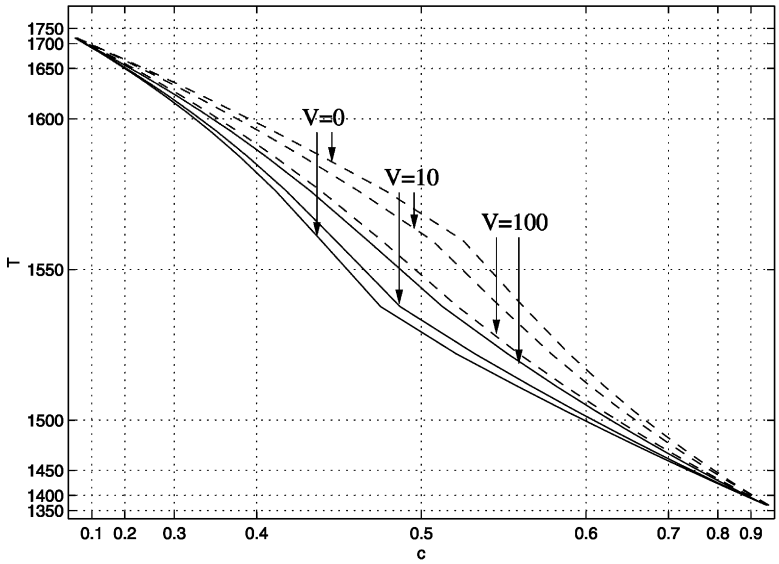

Fig. 4. The kinetic phase diagram for three different growth velocities. The liquidus curves are shown as dashed lines, and the solidus curves as solid lines. As the velocity increases, the curves approach the T_0-line. Note that the scales have been exaggerated to show the difference between curves. The apparent cusps in the figure are only artifacts of this exaggeration.

The continuous growth model of Aziz and Kaplan [3] provides the expression

$$k = \frac{k_e + V/V_\mathrm{d}}{1 + V/V_\mathrm{d}} \tag{7.8}$$

for the partition coefficient of dilute solutions, where V_d is the characteristic velocity associated with solute trapping. For comparison, this function is also shown in Fig. 3. The value for V_d was determined by a least-squares fit. Our computation also agrees quite well with that of Ahmad et al. [1].

As a second example we compute the complete phase diagram for the example above at several different velocities. The results are given in Fig. 4. As the velocity increases, the non-equilibrium liquidus and solidus approach the T_0-line. These computations agree in a qualitative sense with those in Ref. [3].

8. Conclusions

A theory for the rapid solidification of binary alloys has been presented. By a careful consideration of the scales involves, the small interface width analysis allows a precise connection between sharp interface and phase field models to be established. In the case of intermediate velocity scales, it was possible to construct the phase diagram for a wide range of velocities, demonstrating solute trapping effects.

The critical velocity for solute trapping was given in Eq. (2.19). Said differently, this is the scale where the diffusion length in the solid becomes comparable to the interface width, which necessitates a theory which provides descriptions at small scales, such as phase field models do. Note, however, that the crucial aspect of the asymptotic analysis was that that the ratio of diffusion length to interface width was maintained, not merely that the interface width was taken to be small. For purposes of numerical computation this is very important, since it is prohibitively inefficient to use the actual interface width for complex simulations.

The model we have used contains a fair amount of generality, although other phenomenon, such as heat flow and surface energy anisotropy should be included in a realistic model. We do not expect these to change the essence of the analysis, however, since these effects do not typically vary on the interfacial length scale.

Acknowledgements

The author benefited from discussions with Paul Fife, David Eyre and John Cahn.

References

[1] N. Ahmad, A.A. Wheeler, W. Boettinger, G. McFadden, Solute trapping and solute drag in a phase-field model of rapid solidification, Phys. Rev. E 58 (1998) 3436–3450.
[2] M.J. Aziz, W.J. Boettinger, On the transition from the short range diffusion limited to collision limited growth in alloy solidification, Acta Metall. Mater. 42 (1994) 527–537.
[3] M.J. Aziz, T. Kaplan, Continuous growth model for interface motion during alloy solidification, Acta Metall. 36 (1988) 2335–2347.
[4] J.C. Baker, J.W. Cahn, Thermodynamics of Solidification, American Society for Metals, Metals Park, OH, 1971.
[5] Z. Bi, R.F. Sekerka, Phase-field model of solidification of a binary alloy, Physica A 261 (1998) 95–106.
[6] G. Caginalp, P. Fife, Dynamics of layered interfaces arising from phase boundaries, SIAM J. Appl. Math. 48 (1988) 506–518.
[7] G. Caginalp, W. Xie, Mathematical models of phase boundaries in alloys: phase field and sharp interface, Phys. Rev. E 48 (1993) 1897–1909.
[8] C. Charach, P.C. Fife, Solidification fronts and solute trapping in a binary alloy, SIAM J. Appl. Math. 58 (1998) 1826–1851.
[9] J.B. Collins, H. Levine, Diffusion interface model of diffusion limited crystal growth, Phys. Rev. B 31 (1985) 6118.
[10] M. Conti, Heat diffusion and banding in rapid solidification, Phys. Rev. E 58 (1998) 6166–6172.

[11] M. Conti, Transition from dendritic to planar growth and banded structure formation in rapidly solidified alloys, Phys. Rev. E 58 (1998) 6101–6108.
[12] K.R. Elder, F. Drolet, J.M. Kosterlitz, M. Grant, Stochastic eutectic growth, Phys. Rev. Lett. 72 (1994) 677–681.
[13] E. Fried, M.E. Gurtin, Continuum theory of thermally induced phase transitions based on an order parameter, Physica D 68 (1993) 326–343.
[14] E. Fried, M.E. Gurtin, Dynamic solid–solid transitions with phase characterized by an order parameter, Physica D 72 (1994) 287–308.
[15] M. Hillert, B. Sundman, A solute-drag treatment of the transition from diffusion-controlled to diffusionless solidification, Acta Metall. 25 (1976) 11–18.
[16] K.A. Jackson, G.H. Gilmer, H.J. Leamy, Laser and Electron Beam Processing of Materials, Academic Press, New York, 1980, p. 51.
[17] S.G. Kim, W.T. Kim, T. Suzuki, Interfacial compositions of solid and liquid in a phase field model with finite interface thickness for isothermal solidification in binary alloys, Phys. Rev. E 58 (1998) 3316–3323.
[18] J.S. Langer, Models of Pattern Formation in First Order Phase Transitions, World Scientific, Singapore, 1986.
[19] O. Penrose, P. Fife, Thermodynamically consistent models for the kinetics of phase transitions, Physica D 43 (1990) 44–62.
[20] P.M. Smith, M.J. Aziz, Solute trapping in aluminum alloys, Acta Metall. Mater. 42 (1994) 3515.
[21] J. Taylor, J. Cahn, C. Handwerker, Geometric models of crystal growth, Acta. Metall. Mater. 40 (1992) 1–39.
[22] J. Tiaden, B. Nestler, H.J. Diepers, I. Steinbach, The multiphase-field model with an integrated concept for modelling solute diffusion, Physica D 115 (1998) 73–86.
[23] S. Wang, R. Sekerka, A.A. Wheeler, B. Murray, C. Coriell, R. Braun, G. McFadden, Thermodynamically consistent phase-field models for solidification, Physica D 69 (1993) 189–200.
[24] J.A. Warren, W.J. Boettinger, Prediction of dendritic growth and microsegregation patterns in a binary alloy using the phase field method, Acta Metall. Mater. 43 (1995) 689–703.
[25] A.A. Wheeler, W. Boettinger, G. McFadden, Phase-field model for isothermal transitions in binary alloys, Phys. Rev. A 45 (1992) 7424–7439.
[26] A.A. Wheeler, W. Boettinger, G. McFadden, Phase-field model of solute trapping during solidification, Phys. Rev. E 47 (1993) 1893–1909.
[27] A.A. Wheeler, W. Boettinger, G. McFadden, Phase-field model for solidification of a eutectic alloy, Proc. R. Soc. A 452 (1996) 495.